© 2022. Published by The Company of Biologists Ltd | Development (2022) 149, dev200419. doi:10.1242/dev.200419

STEM CELLS AND REGENERATION

RESEARCH ARTICLE

Embryonic vascular establishment requires protein C receptor-expressing endothelial progenitors

Qing Cissy Yu[1,*,‡], Lanyue Bai[1,*], Yingying Chen[1,*], Yujie Chen[3], Guangdun Peng[4], Daisong Wang[1], Guowei Yang[2], Guizhong Cui[4], Naihe Jing[1,4,5,‡] and Yi Arial Zeng[1,2,‡]

ABSTRACT

Vascular establishment is one of the early events in embryogenesis. It is believed that vessel-initiating endothelial progenitors cluster to form the first primitive vessel. Understanding the molecular identity of these progenitors is crucial in order to elucidate lineage hierarchy. In this study, we identify protein C receptor (Procr) as an endothelial progenitor marker and investigate the role of Procr^{+} progenitors during embryonic vascular development. Using a *Procr*$^{mGFP\text{-}2A\text{-}lacZ}$ reporter, we reveal a much earlier *Procr* expression (embryonic day 7.5) than previously acknowledged (embryonic day 13.5). Genetic fate-mapping experiments using *Procr*^{Cre} and *Procr*^{CreER} demonstrate that Procr^{+} cells give rise to blood vessels throughout the entire embryo proper. Single-cell RNA-sequencing analyses place Procr^{+} cells at the start of endothelial commitment and maturation. Furthermore, targeted ablation of Procr^{+} cells results in failure of vessel formation and early embryonic lethality. Notably, genetic fate mapping and scRNA-seq pseudotime analysis support the view that Procr^{+} progenitors can give rise to hemogenic endothelium. In this study, we establish a Procr expression timeline and identify Procr^{+} vessel-initiating progenitors, and demonstrate their indispensable role in establishment of the vasculature during embryo development.

KEY WORDS: Procr, Endothelial progenitor, Vessel initiation, Fate mapping, Embryonic vessel, Mouse

INTRODUCTION

Vascular development is one of the earliest organogenesis events in development. Vascular architecture provides a travel route for circulating cells and ensures the delivery of nutrients. Endothelial cells (ECs) are the major functional units, which form a continuous monolayer lining all vessels. EC differentiation occurs during gastrulation when cells invaginate through the primitive streak (PS) to form mesoderm (Eichmann et al., 2005). Blood vessel organization in the embryo proper and yolk sac is initiated by aggregating angioblasts/endothelial precursors into a primitive plexus (vasculogenesis), followed by complex processes of angiogenesis and vessel remodeling until a functional circulatory system is established (Adams and Alitalo, 2007; Carmeliet, 2003; Coultas et al., 2005; Ema and Rossant, 2003). Understanding of the events surrounding endothelial lineage commitment or early vessel initiation remains incomplete, and the identification of molecular markers for these progenitors would aid further elucidation of these processes.

Protein C receptor (Procr, also known as EPCR, CD201) is a single-pass transmembrane receptor protein with well-established roles in anti-coagulation regulation and cytoprotection (Fukudome and Esmon, 1995; Griffin et al., 2012; Mohan Rao et al., 2014). By binding to its primary ligand, protease precursor protein C (PC), Procr increases the generation of activated PC (aPC). The Procr-PC pathway modulates thrombin generation through the degradation of clotting factors VIIIa and Va (Esmon et al., 1999; Griffin et al., 2012; Mohan Rao et al., 2014). Aside from participation in anti-coagulation, studies have also shown that binding of PC to Procr elicits anti-apoptotic, anti-inflammatory and cytoprotective responses that ensure vascular homeostasis (Cheng et al., 2003; Esmon, 2001).

More recently, Procr has been reported to mark adult stem cells in multiple tissues (Balazs et al., 2006; Fares et al., 2017; Wang et al., 2015; Yu et al., 2016), including the resident stem cells of hematopoietic (Fares et al., 2017; Ye et al., 2017; Zhou et al., 2016) and adult vascular system (Yu et al., 2016). However, whether Procr has a role during early embryonic vascular formation or later-occurring hematopoiesis remains unclear so far. In the mouse embryo, definitive hematopoietic stem cells (HSCs) emerge around mid-gestation at embryonic day (E) 10.5 (Clements and Traver, 2013; Li et al., 2012; Zovein et al., 2008). A temporal sequencing study over the course of HSC emergence identified *Procr* as one of the genes highly expressed in pre-HSCs (Zhou et al., 2016), suggestive of a possible role of Procr in HSC generation.

Previous studies have described Procr expression on trophoblast giant cells of the placenta; in the embryo, Procr was first detected on the large vessel of the developing embryo at E13.5 (Crawley et al., 2002). Embryos with homozygous deletion of *Procr* show lethality prior to E10.5 (Gu et al., 2002; Wang et al., 2015). Given that Procr expression was not detected in the early embryo proper, together with the observed excessive fibrin deposition in the maturing placenta, the lethality phenotype in *Procr*$^{-/-}$ embryos has been largely attributed to a placental coagulation defect (Gu et al., 2002). However, a study revealing Procr-expressing pre-HSCs residing in

[1]State Key Laboratory of Cell Biology, CAS Center for Excellence in Molecular Cell Science, Institute of Biochemistry and Cell Biology, University of Chinese Academy of Sciences, Chinese Academy of Sciences, Shanghai 200031, China. [2]School of Life Science, Hangzhou Institute for Advanced Study, University of Chinese Academy of Sciences, Chinese Academy of Sciences, 310024 Hangzhou, China. [3]Key Laboratory of Computational Biology, CAS-MPG Partner Institute for Computational Biology, Shanghai Institute of Nutrition and Health, Shanghai Institutes for Biological Sciences, University of Chinese Academy of Sciences, CAS, Shanghai 200031, China. [4]CAS Key Laboratory of Regenerative Biology, Guangdong Provincial Key Laboratory of Stem Cell and Regenerative Medicine, Guangdong Institutes of Biomedicine and Health, Chinese Academy of Sciences, Guangzhou 510530, China. [5]Institute for Stem Cell and Regeneration, Chinese Academy of Sciences, Beijing 100101, China.
*These authors contributed equally to this work

‡Authors for correspondence (cissyyu@sibcb.ac.cn; njing@sibcb.ac.cn; yzeng@sibcb.ac.cn)

Q.C.Y., 0000-0001-7516-7137; Yingying Chen, 0000-0002-0243-8730; N.J., 0000-0003-1509-6378; Y.A.Z., 0000-0003-1898-8099

Handling Editor: Liz Robertson
Received 30 November 2021; Accepted 5 May 2022

Development (2022) 149, dev200419. doi:10.1242/dev.200419

the AGM of E10.5/E11.0 embryos (Zhou et al., 2016) contradicts the reported lack of Procr expression in the embryo before E13.5 (Crawley et al., 2002). These conflicting pieces of evidence prompted us to re-examine the expression pattern of Procr and to investigate its potential role during early embryonic development.

In this study, we identify a population of endothelial progenitors marked by Procr expression during early vessel formation. By lineage tracing, single-cell RNA sequencing (scRNA-seq) and targeted Procr^{+} cell ablation, we show that Procr^{+} endothelial progenitors are essential for establishment of the vasculature and provide evidence that Procr^{+} endothelial progenitors contribute to hemogenic endothelium.

RESULTS

Procr expression is detected on the forming vasculature of the early embryo

The murine *Procr* gene spans 8.8 kb and is composed of four exons and three introns (Fukudome and Esmon, 1995). To investigate *Procr* expression during early embryogenesis, we employed a knock-in reporter allele, in which an *mGFP-2A-lacZ* cassette was inserted after the ATG of the *Procr* gene (Fig. 1A) (Wang et al., 2020). X-gal staining of the *Procr*$^{mGFP\text{-}2A\text{-}lacZ/+}$ embryo indicated extra-embryonic Procr expression prior to primitive streak migration: at E7.0-E7.5, Procr expression was concentrated at extra-embryonic ectoderm, especially at the feto-maternal boundary (Fig. 1B,C). We first detected *Procr* expression in the embryo proper at E7.5, alongside the migrating streak (Fig. 1C, black arrow). To strengthen our *in vivo* observation, we analyzed the transcriptional expression of *Procr* using published single-cell RNA-sequencing data on E7.5 whole embryo (Pijuan-Sala et al., 2019), which also shows enriched *Procr* expression in the cell clusters 'hematoendothelial progenitors' (Fig. 1C, right panel). At E7.75, *Procr* expression was detected at the ventral side of the migrating streak (Fig. 1D,D′). At E8.0-E8.25, when the neural fold at the anterior endoderm region is visibly structured, the expression of *Procr* was concentrated at the site of the forming aorta

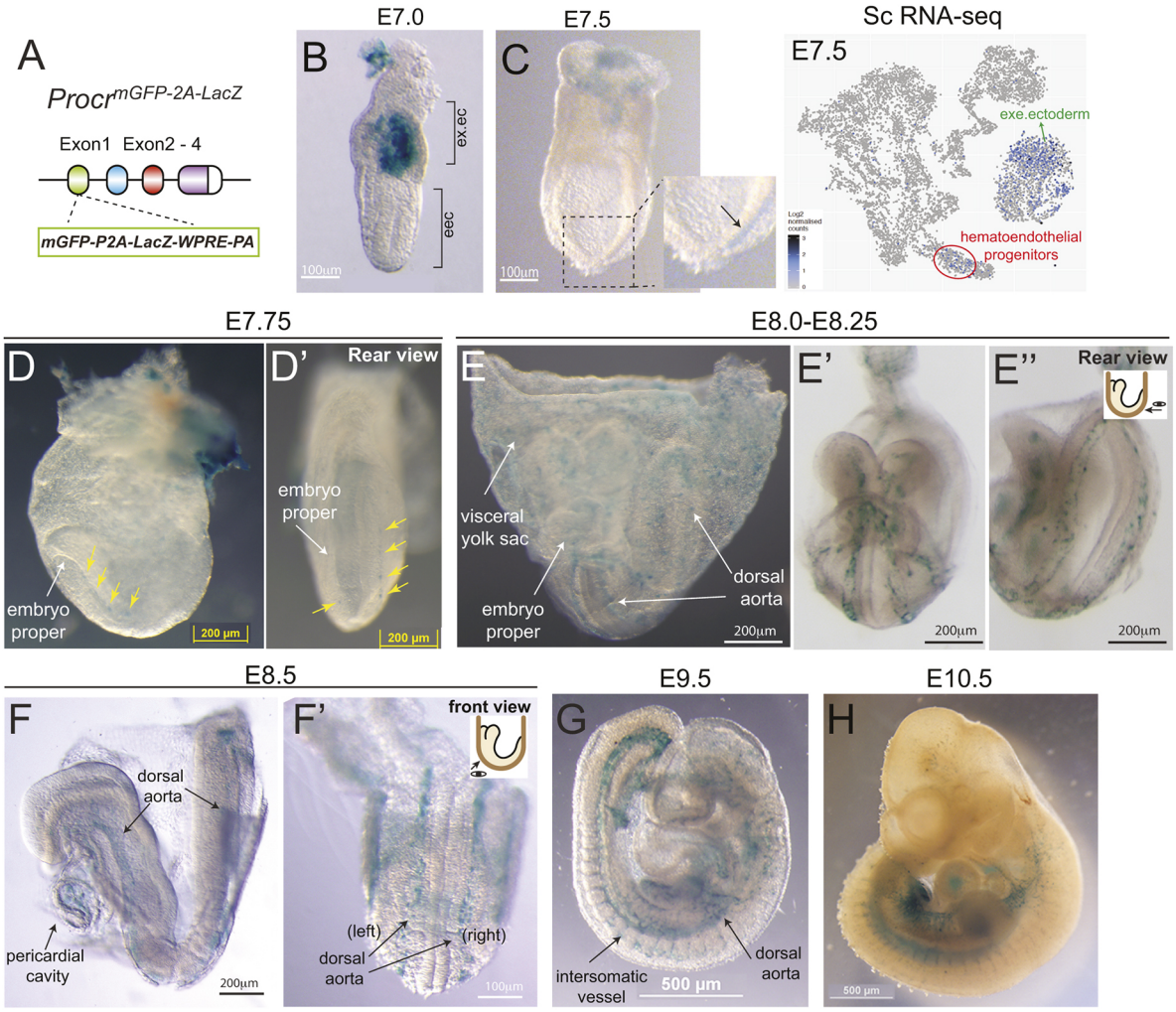

Fig. 1. Procr^{+} cells detected in the forming vasculature during early embryonic development. (A) Illustration of the knock-in strategy for constructing the *Procr*$^{mGFP\text{-}2A\text{-}lacZ}$ model. (B-H) X-gal staining of the *lacZ* reporter was performed on *Procr*$^{mGFP\text{-}2A\text{-}lacZ}$ embryos to characterize Procr expression. (B) At E7.0, strong *lacZ* signals were detected in the extra-embryonic ectoderm. eec, embryonic ectoderm; ex.ec, extra-embryonic ectoderm. (C) Left: Procr expression in the embryo proper first appears at E7.5. Inset shows magnification of the boxed area. Black arrow indicates β-galactosidose staining (*lacZ* expression). Single-cell sequencing of E7.5 embryos shows that Procr is highly expressed in the 'hematoendothelial progenitor' population. exe. ectoderm, extra-embryonic ectoderm. (D-F′) From E7.75 to E8.5, Procr expression is detected at the forming left and right dorsal aorta of the embryo proper, as indicated by arrows. Insets in E″ and F′ show schematics indicating the view shown in the respective images. Arrow and eye indicate the direction of view. (G,H) As development proceeds, expression of Procr is closely associated with sites of forming vascular beds. Embryos from the same pregnant female were harvested and stained together. Embryos from more than three pregnant female mice were analyzed for each time point.

Development (2022) 149, dev200419. doi:10.1242/dev.200419

(Fig. 1E-E″), which was also confirmed using whole-embryo *in situ* hybridization (Fig. S1A). By E8.5, *Procr-lacZ* signals outlined both left and right dorsal aorta throughout the embryo proper (Fig. 1F,F′), and robust Procr expression was also detected inside the pericardial cavity (Fig. 1F). We performed fluorescence-activated cell sorting (FACS) analysis on E8.25 embryos and found that Procr is expressed in about 4-5% of all CD31 (PECAM1)-expressing ECs (Fig. S1B). At E9.5, *Procr* expression was found on major intersomatic vessels in addition to the dorsal aorta (Fig. 1G). Scattered β-galactosidose staining (reflecting *lacZ* expression, and therefore Procr expression) was observed at AGM region, and the area surrounding the gut tube. At E10.5 onwards, β-galactosidose expression was detected at sites of robust vascular expansion, including thoracic vessels, ventral skin vascular plexus and cranial vessels (Fig. 1H). X-gal staining of the wild-type embryos showed no nonspecific β-galactosidose staining (Fig. S2A).

X-gal staining of the E8.5 $Procr^{mGFP\text{-}2A\text{-}lacZ/+}$ embryo revealed a specific expression pattern of Procr on the forming dorsal aorta (Fig. 1F,F′). To validate this, we inspected the distribution of $Procr^{+}$ cells by staining for the mGFP reporter signal in the $Procr^{mGFP\text{-}2A\text{-}lacZ/+}$ model. At E8.5, co-staining with the endothelial marker CD31 or ERG (which labels endothelial nuclei), we found that *Procr* was expressed in an endothelial subpopulation of the expanding aorta, which is the first major vessel to form during embryonic development (Fig. S1C,D, white-boxed area shown as higher magnification). One day later, at E9.5, $Procr^{+}$ cells were detected on the forming vascular plexus of multiple locations, including the AGM region (Fig. S1E) and the endothelial linings of emerging intersomatic vasculature (Fig. S1F).

The expression pattern of Procr throughout early to mid-stages of embryonic proper development coincides with sites of vessel initiation and robust vascular expansion activities. Online spatial transcriptome analysis (GEO-seq) also supported the notion. In GEO-seq, cells at a defined anatomical position of E6.5 and E7.5 embryos were captured by laser microdissection, followed by transcriptome analyses (Peng et al., 2016). With spatial gene expression displayed as a corn plot, we found that the very first *Procr*-expressing cells within the embryo proper emerge at the migrating posterior mesoderm, before the onset of CD31 expression, a marker for mature endothelial lineage (Fig. S2B-D).

Together, these data suggest that the expression of *Procr* in embryo proper is much earlier than E13.5 as previously reported. Moreover, the emergence of $Procr^{+}$ cells in the early embryo coincided with the sites of vessel initiation, suggesting that $Procr^{+}$ ECs may constitute first formed vessels.

$Procr^{+}$ endothelial progenitors contribute to developing vasculature

Next, we set to investigate whether these $Procr^{+}$ cells are endothelial progenitors by *in vivo* lineage tracing. To this end, we used a recently constructed *Procr-Cre* knock-in allele and generated $Procr^{Cre}$;$R26^{LSL\text{-}tdTomato}$ mice by genetic crossing (Fig. 2A, Fig. S3A,B). *Procr* expression results in activation of tdTomato expression in $Procr^{+}$ cells, which would be passed on to all of their progeny (Fig. 2A). This constitutively active $Procr^{Cre}$ line allows sensitive detection of Procr expression in early development, without relying on tamoxifen (TAM) induction efficiency. $tdTomato^{+}$ signal was first detected at E7.5 in $Procr^{Cre}$;$R26^{LSL\text{-}tdTomato}$ embryos, with individually labeled $Procr^{+}$ cells located at both the extra-embryonic endoderm (labeled as tdTomato ex.en), and inside the migrating primitive streak (labeled as tdTomato PS) (Fig. 2B), which is in accordance with GEO-seq analysis results indicating their first emergence at the mesoderm side of the migrating streak (Fig. S2B-D).

To assess the fate of Procr-expressing ECs, $Procr^{Cre}$;$R26^{LSL\text{-}tdTomato}$ embryos were evaluated at E12.5. Immunostaining revealed that $Procr^{+}$ cells and their descendants had actively contributed to the formation of vascular beds at various organ sites (Fig. 2C). By co-staining with the endothelial markers CD31 or ERG, we observed densely, if not entirely, $tdTomato^{+}$ vessels at various locations, including the vessel plexus around the forming cranial vessels (Fig. 2D) and large vessels (Fig. 2E), in the descending aorta next to the forming spine (Fig. 2F), throughout the intersomatic vessels (Fig. 2G), in the vessel plexus of forming mesentery (Fig. 2H), as well as alongside the tail segments (Fig. 2I). In parallel, we also employed a $Procr^{CreERT2}$ knock-in mouse model (Wang et al., 2015), and crossed with $Rosa26^{LSL\text{-}tdTomato}$ to obtain an inducible reporter of Procr-expressing cells. Pregnant mice were injected with TAM at E8.5 and embryos were harvested at E12.5 for analysis (Fig. 2J). Co-staining with ERG confirmed the presence of $tdTomato^{+}$ ECs throughout the embryo vasculature, including intersomatic vessels (Fig. 2K) and large vessels (Fig. 2L). To evaluate the induction efficiency of the $Procr^{CreERT2}$;$R26^{LSL\text{-}tdTomato}$ model, we administered TAM to pregnant females at E8.5, and harvested embryos at E10.5 (Fig. S3C). After genotyping, $Procr^{CreERT2}$;$R26^{LSL\text{-}tdTomato}$ embryos were individually digested and analyzed by FACS. As shown, 28.4±4.5% of $CD31^{+}$ $Procr^{+}$ cells were $tdTomato^{+}$ (Fig. S3E), reflecting the $Procr^{CreERT2}$ labeling efficiency, and 18.3±1.4% $CD31^{+}$ $tdTomato^{+}$ cells were $Procr^{+}$ (Fig. S3F), reflecting progeny generation from $Procr^{+}$ progenitors. These lineage-tracing findings suggest that Procr labels endothelial progenitors that generate embryonic vasculature of the embryo proper.

$Procr^{+}$ ECs contribute to yolk sac and placental vasculature

When analyzing the expression pattern of *Procr* using $Procr^{mGFP\text{-}2A\text{-}lacZ}$, we noticed *Procr* expression on the forming vessels of the visceral yolk sac (see Fig. 1E). Closer examination at E10.5 revealed strong β-galactosidose staining on the expanding vessels throughout visceral yolk sac (Fig. S4A). Expression of Procr was also present in developing placenta as previously reported. Initially, Procr was detected on embryonic trophectoderm-derived giant cells at the interface between maternal and embryonic tissues (Fig. 1B,C), which is consistent with a previous report using Procr immunofluorescent antibody staining (Crawley et al., 2002).

To assess the contribution of $Procr^{+}$ cells towards vasculature of visceral yolk sac and placenta, we performed lineage-tracing experiments using the $Procr^{Cre/+}$;$Rosa26^{LSL\text{-}mTmG/+}$ line, in which $Procr^{+}$ cells and their descendants are marked by mGFP expression. Vascular networks for the visceral yolk sac and the embryonic side of the placenta are well established by E16.5. Using whole-mount immunostaining, we found that most of the established vessels were lined by $mGFP^{+}$ ECs (Fig. S4B,C), indicating that $Procr^{+}$ cells contribute robustly to the formation of the inter-woven visceral vasculature, including both venous (Fig. S4B) and arterial branches (Fig. S4C).

Starting at E9.5, trophoblasts, with their associated fetal blood vessels, undergo extensive villous branching to create a tortuous and densely packed structure termed the labyrinth. The labyrinth provides direct contact between maternal blood and fetal trophoblastic villi, ensuring ease of material exchange between the two blood systems (Rossant and Cross, 2001). By co-staining with collagenase IV, an endothelial basement membrane marker used to outline vessel structure, we also found that the labyrinth of

Development (2022) 149, dev200419. doi:10.1242/dev.200419

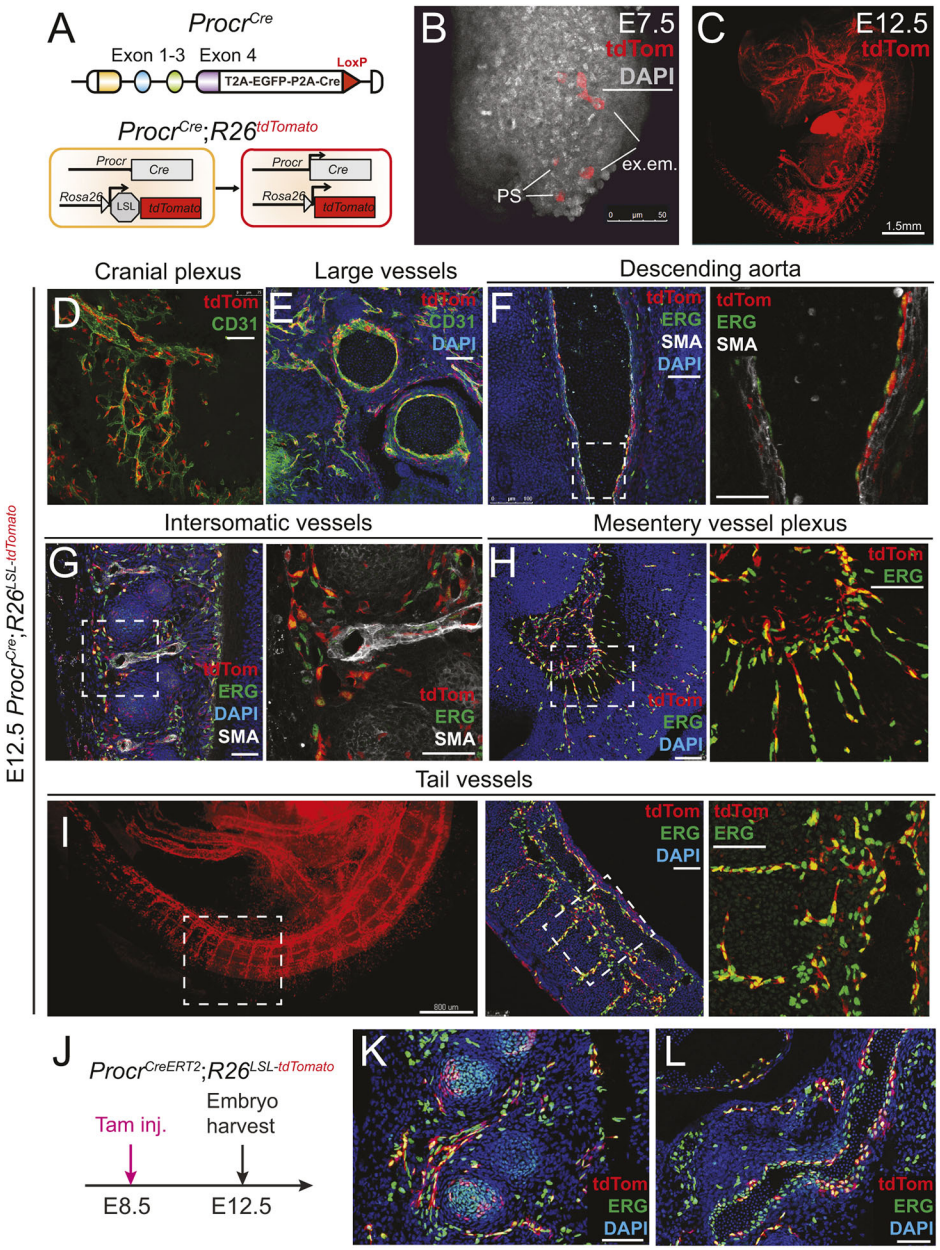

Fig. 2. Procr$^+$ cells contribute to vascular development. (A) Schematic of *Procr^{Cre}* knock-in allele generation (see also Fig. S3) and lineage-tracing strategy using the *Procr^{Cre};R26$^{LSL\text{-}tdTomato}$* line. (B) Image showing the earliest detection of tdTomato$^+$ (Procr$^+$) cells in the E7.5 embryo. tdTom, tdTomato. Scale bar: 50 µm. (C) Image of E12.5 a *Procr^{Cre};R26$^{LSL\text{-}tdTomato}$* whole embryo (also see Movie 1). (D-I) Representative images showing lineage tracing of Procr$^+$ ECs, which identified their major contribution to various vascular beds, including vessel plexus of the cranial vessel (D), large vessels (E), descending aorta (F), intersomatic vessels (G), mesentery vessel plexus (H) and tail vessels (I). The boxed area in each image is enlarged on the right. CD31 marks the endothelial surface. ERG marks endothelial nuclei. SMA, α smooth muscle actin. DAPI, 4′,6-diamidino-2-phenylindole. Scale bars: 50 µm. (J) Illustration of the lineage-tracing strategy of Procr$^+$ cells using the *R26$^{LSL\text{-}tdTomato}$* reporter. Pregnancy was timed and TAM administered at E8.5. Embryos were harvested at E12.5. (K,L) Representative embryo sections showing tdTomato$^+$ ERG$^+$ ECs at intersomatic vessels (K) and large vessels (L). Scale bars: 75 µm. Embryos from at least three pregnant female mice were analyzed in each lineage-tracing experiment.

the placenta was heavily laced with GFP$^+$ vessel structure (Fig. S4D). Together, these lineage-tracing results suggest that Procr$^+$ cells contribute to the expanding vasculature of the developing yolk sac and placenta.

scRNA-seq and lineage tracing reveal that Procr$^+$ progenitors are the cellular origin of endothelial lineages

To understand further the cellular evolutions and molecular events that occur during endothelial specification, we investigated the transcriptome characteristics of Procr$^+$ cells at early vasculature formation using single-cell sequencing (scRNA-seq) analysis (Fig. 3A). We analyzed a published dataset on Flk1 (also known as KDR and VEGFR2)$^+$ EC progenitors and their progeny from E8.25 embryos (Pijuan-Sala et al., 2019), together with our new dataset using FACS-isolated CD31$^+$ ECs from E8.5 and E10.5 embryos. We also included FACS-isolated CD45 (PTPRC)$^+$ hematopoietic cells from E10.5 embryo in the analysis, because blood-generating hemogenic endothelium and endothelial progenitors are known to share many molecular features (Zhou et al., 2016). On average, we detected 7940 genes and 1,116,770 counts expressed in each individual cell (Fig. S5A). After principal component analysis (PCA), dimensional reduction and cell clustering, the combined datasets can be separated into 11 clusters (Fig. 3B, Fig. S5B). Together with their sampling stages (Fig. 3C) and marker expression (Fig. 3D, Fig. S5C,D), we annotated each population as early-developing ECs (clusters 1 and 2 from E8.25 and cluster 3 from E8.5), late-mature ECs (clusters 4 and 5 from E10.5), mesenchymal-like cells (clusters 6 and 7), erythrocytes (cluster 8), ECs with hematopoietic properties (labeled as hematopoietic-primed ECs, cluster 9), and CD45$^+$ hematopoietic cells (clusters 10 and 11).

Trajectory analysis by Monocle 2 identified E8.25 Procr$^+$ progenitors as the starting population along developmental pseudotime, from which two bifurcations form as cells commit towards either endothelial or blood fates (Fig. 3E, Fig. S5E,F). Consistent with previous studies, EC maturation path is accompanied by the expression of key transcription factors (TFs) for endothelial

Development (2022) 149, dev200419. doi:10.1242/dev.200419

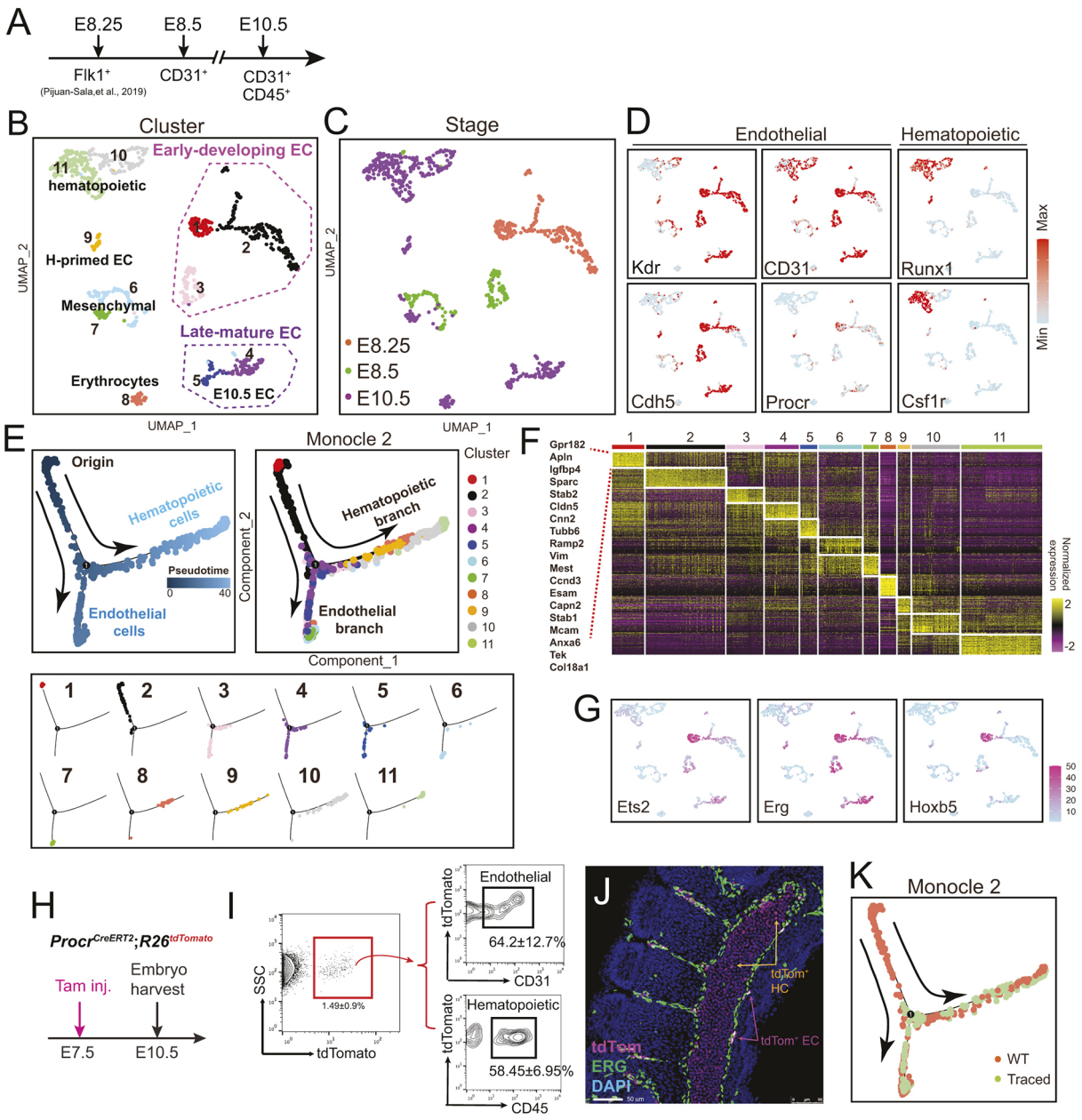

Fig. 3. scRNA-seq reveals that Procr^{+} progenitors could give rise to both endothelial and hematopoietic lineages. (A) Illustration of sample collection time points. The E8.25 time point applies to the dataset previously published by Pijuan-Sala et al. (2019). (B) UMAP plot of scRNA-seq profiles, colored by cluster assignment. H-primed EC, hematopoietic-primed ECs. (C) UMAP plot of cells colored by cell stages. (D) Individual gene UMAP plots showing the expression levels and distribution of representative marker genes of known endothelial and hematopoietic cell types. The colors ranging from blue to red indicate low to high relative gene expression levels. (E) Developmental trajectory of cells generated by Monocle 2. Pseudotime (arbitrary units) is depicted from dark to light blue (left). The colors in the right panel denote cell types. Both merged (top) and split (bottom) views are shown. (F) Heatmap of cell type-enriched genes. Each column represents a single cell and each row represents one signature gene. The colors ranging from purple to yellow indicate low to high relative gene expression levels. (G) UMAP plots showing the differential activation levels of TFs in each cluster. Colors from light blue to magenta indicate low to high activities of the TFs. (H) Pregnancy was timed and TAM administered (0.5 mg/25 g body weight) at E7.5. Embryos were harvested at E10.5. (I) FACS analysis of Procr^{+} cell progeny in E10.5 embryos. In whole-embryo single cells, 1.49±0.9% of cells are tdTomato^{+}. Within all tdTomato^{+} cells, 64.2±12.7% of cells are CD31^{+} and 58.45±6.95% of cells are CD45^{+}. Data in FACS plots are from at least five embryos and presented as mean±s.e.m. (J) Representative confocal images of *Procr*^{CreERT2};*R26*^{tdTomato} traced embryos immunostaining, indicating that tdTomato^{+} population comprises ERG^{+} ECs and blood cells within vessels. (K) Developmental trajectory of cells generated by Monocle 2, colored by wild-type (WT)/traced cells. (H-J) Induced lineage tracing experiments were performed using three pregnant female mice and at least 20 embryos were examined.

commitment, including *Etv2*, *Ets1*, *Ets2*, *Sox7* and *Sox17*, as well as the gradual onset of arterial and venous specification [arterial: *Gja5* (Buschmann et al., 2010); venous: *Nr2f2*, *Ltbp4* (Swift et al., 2014)] (Fig. S5G). Along the EC maturation path, hematopoietic potentiated ECs segregated out as early as E8.5 (cluster 3), which is characterized by the switching on of hematopoietic TFs, including *Runx1*, *Spn* and *Adgrg1* (Fig. S5H).

To determine the transcriptome signature of Procr^{+} progenitors, we performed transcriptome clustering of all populations and showed that Procr^{+} progenitors display patterned genes (i.e. a

Development (2022) 149, dev200419. doi:10.1242/dev.200419

unique expression pattern of genes), including *Apln*, *Gpr182*, *Igfbp4*, *Cldn5*, *Cnn2*, *Ramp2*, *Ccnd3*, *Mcam*, *Tek* and *Col8a1* (Fig. 3F). To understand better the molecular regulation of Procr^{+} progenitors during endothelial commitment, we analyzed TF activities from patterned genes in E8.25 Procr^{+} progenitors. We found previously reported key regulators of endothelial lineage specification, including *Ets2* and *Erg*, with target genes activities that significantly overlapped with the patterned genes identified in our transcriptome analysis. We also identified a core TF, *Hoxb5*, which is highly active specifically in the Procr^{+} progenitor cluster (Fig. 3G). Given the simultaneous high activities of Hoxb5 and its predicted target genes, including *Hoxb5*, *Maf*, *Slk* and *Adam12* (Fig. S5I), *Hoxb5* is likely a core TF during endothelial specification.

The pseudotime trajectory identified Procr^{+} progenitors as the cellular origin of both endothelial and hematopoietic cells (Fig. 3E). To validate these two fate commitments of Procr^{+} cells *in vivo*, we used the *Procr*^{CreERT2};*R26*^{tdTomato} inducible reporter. To ensure efficiency of induction, timed pregnant female mice were treated with TAM at E7.5, and embryos were harvested at E10.5 (Fig. 3H). FACS analysis of traced tdTomato-expressing cells indicated the presence of both endothelial (CD31^{+}, tdTomato^{+}) and hematopoietic (CD45^{+}, tdTomato^{+}) populations (Fig. 3I), which was also confirmed by immunofluorescence staining (Fig. 3J). To verify the identity of traced tdTomato^{+} cells, we isolated E10.5 tdTomato^{+} cells by FACS and performed scRNA-seq. By integrated analysis of traced (tdTomato^{+}) cells with wild-type cells, Monocle 2 analysis showed that tdTomato^{+} cells were present in both the endothelial and hematopoietic branches, validating the suggestion that early labeled Procr^{+} progenitors give rise to both endothelial and hematopoietic cells (Fig. 3K).

Procr^{+} cell ablation results in lethal vascular defects of the embryo

To assess the functional importance of Procr^{+} cells during vascular initiation, we performed targeted cell ablation in the developing embryo. We generated *Procr*^{CreERT2};*R26*$^{DTA/+}$ mice to conditionally express diphtheria toxin (DTA) in Procr^{+} cells upon TAM induction (Fig. 4A). This allowed us to determine the role of Procr^{+} cells in development. TAM was administered prior to E8.5 and at E10.5, and the effect on embryos was analyzed at E13.5 (Fig. 4B). Ablation of Procr^{+} cells at such an early stage led to lethality, with severe vessel leakage in the placenta and much smaller embryos compared with control (*R26*$^{DTA/+}$) (Fig. 4C). When analyzing the embryo proper, we found that *Procr*^{CreERT2};*R26*$^{DTA/+}$ embryos morphologically barely mature beyond E9.5 (Fig. 4D, three embryos on the right), and appeared pale in color, indicative of an underdeveloped or dysfunctional circulation system. We also noticed vasculature establishment failed at both the visceral yolk sac and the placenta, and the embryo proper was disconnected from its placenta, because connecting cord blood vessels failed to form between the embryo and the placenta (Fig. 4E,F). To determine the time course for lethality, we administered TAM to pregnant mice at E7.5 and E8.5, and collected embryos at different time points (Fig. S6A). We found that at E10.5 *Procr*^{CreERT2};*R26*$^{DTA/+}$ embryos were drastically smaller compared with control (Fig. S6B). By E11.5, the *Procr*^{CreERT2};*R26*$^{DTA/+}$ embryos turned opaque and displayed deformity at multiple sites, including the head and limbs, as well as a lack of active circulation (Fig. S6C). These observations suggest that the lethality time window is around E10.5-E11.5.

Immunofluorescence staining of E13.5 whole embryo sections confirmed the drastic reduction of CD31^{+} endothelial cells upon ablation of Procr-expressing cells compared with control (Fig. 4G,H). We chose sagittal sections in order to display the majority of the organs. Whereas the control displayed rich vascular penetration into most developing body parts (Fig. 4G), Procr^{+} cell ablation led to sparse CD31^{+} staining at the AGM region, with other body parts largely avascular (Fig. 4H, enlarged view). In addition, ablation of Procr^{+} cells also induced defective vasculature in the visceral yolk sac, as shown by whole-mount staining (Fig. 4I,J). At E13.5, control displayed a hierarchically organized network of the vasculature (Fig. 4I), whereas Procr^{+} cell ablation resulted in fragmented and loosely associated vascular structure (Fig. 4J). In the placenta attaching *Procr*^{CreERT2};*R26*$^{DTA/+}$ embryos, immunostaining of 50-µm-thick placenta sections revealed a complete absence of embryonic labyrinth structure, which is essential for material and oxygen exchange between the maternal circulation and that of the fetus (Fig. 4K-M). These results highlight that Procr^{+} progenitors are essential for the vascular development of the embryo proper, the visceral yolk sac and the placenta.

DISCUSSION

Vascular establishment is a crucial event in early embryogenesis. However, the identity of vessel-initiating endothelial progenitors remains elusive. In the present study, we identify Procr expression during early embryonic vascularization, and demonstrate progenitor properties of Procr^{+} cells by lineage tracing.

Blood vessel organization in the embryo proper and yolk sac is initiated by endothelial precursors aggregating into a primitive plexus (vasculogenesis), followed by complex processes of angiogenesis and vessel remodeling (Adams and Alitalo, 2007; Carmeliet, 2003; Coultas et al., 2005; Ema and Rossant, 2003). Previous studies using Procr antibody staining were not able to detect Procr expression in the embryo proper until E13.5, at which time point weak staining in the aortic endothelium was seen (Crawley et al., 2002; Gu et al., 2002). This discrepancy in Procr expression is probably due to insensitivity of the antibody. In the current study, using a reporter model, *Procr*$^{mGFP\text{-}2A\text{-}lacZ}$, we detected Procr^{+} (*lacZ*$^{+}$) cells in the migrating primitive streak at as early as E7.5. Post-gastrulation staining of *Procr*$^{mGFP\text{-}2A\text{-}lacZ}$ embryos identified a specific vascular distribution from E8.0 to E9.5, which coincides with vascular initiation. Fate mapping of these Procr^{+} cells revealed that their descendants contribute significantly to establishment of the vasculature throughout the entire embryo. Subsequently, at E10.5, we detected *Procr* expression on embryonic endothelial cells in the labyrinthine zone underlying the chorionic plate, indicating that Procr^{+} ECs also contribute towards placental vessels. Given that Procr expression was detected on vessel-initiating endothelium, and Procr^{+} cells actively contributed towards subsequent vessel generation shown by *in vivo* lineage tracing, we propose that Procr labels endothelial progenitor cells at the initiation of vascular morphogenesis.

Although we cannot rule out the possibility that other non-Procr-expressing sources of endothelial vasculature exist, the extensive Procr^{+} cell-driven tracing observed in blood vessels throughout the entire embryo strongly supports the notion that the Procr^{+} progenitor pool is the dominant contributor to the endothelial cell lineage. The targeted ablation experiments further demonstrate the essential role of Procr^{+} progenitor cells. When Procr^{+} cells were ablated at the onset of vessel formation (E8.5), embryonic development seemed to cease shortly after, with an absence of major blood vessels in the embryonic proper, missing cord vessels connecting to the placenta and dysfunctional, tortuous vessels distributed in the visceral yolk sac.

Development (2022) 149, dev200419. doi:10.1242/dev.200419

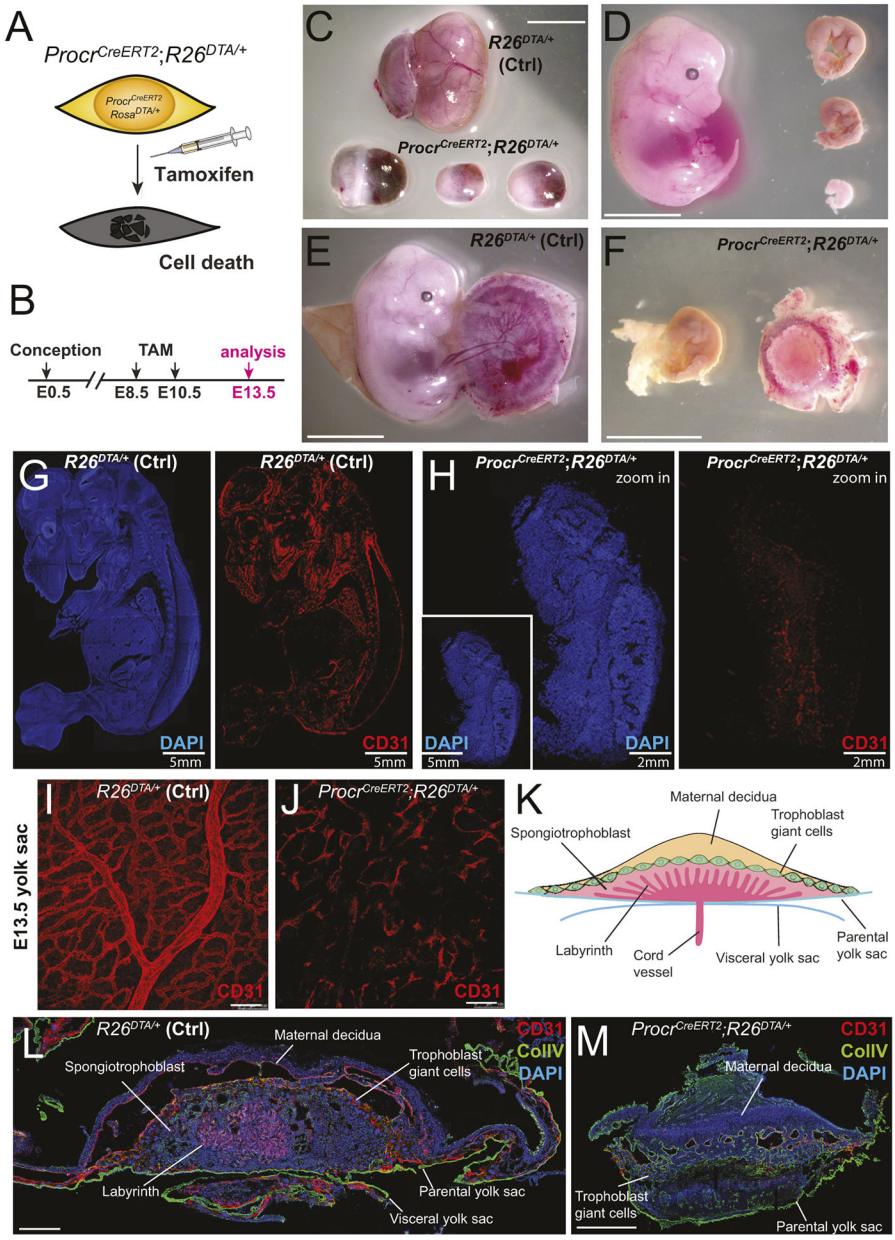

Fig. 4. Ablation of Procr^{+} cells in early embryos stalls vessel development. (A) Schematic of the Procr^{+} cell-ablation strategy using the *Procr*^{CreERT2};*R26*$^{DTA/+}$ line. (B) TAM was administered at E8.5 and E10.5 by maternal peritoneal injection, and the uterus was dissected on E13.5 for embryo morphology analysis. (C-F) Loss of Procr^{+} cells caused severe bleeding of the embryonic facet of the placenta (C) and embryo death. The development of *Procr*^{CreERT2};*R26*$^{DTA/+}$ embryos stalled at around E9.5, and some embryos were in the process of being resorbed (D). Major vessels connecting embryo proper to both the placenta and the visceral yolk sac were missing (E,F). (G-J) Representative images of whole-embryo sections indicate a severe vascular defect in both the embryo proper (G,H) and the visceral yolk sac (I,J). (K) Illustration of the main placental components. (L) Immunofluorescence staining revealed anatomical sites of major components in placenta sections. (M) Ablation of Procr^{+} cells resulted in failed formation of the labyrinth structure. CollV, collagenase IV. Targeted ablation experiments were performed in at least five pregnant female mice. Scale bars: 500 µm (C-F); 100 µm (I,J); 1 mm (L,M).

The embryonic lethality of *Procr* knockout mice has been reported previously (Gu et al., 2002; Wang et al., 2015). Knockout of *Procr* alleles causes embryonic lethality at around E10.5, largely attributed to massive hemorrhaging and thrombosis at the materno-feto interface, severely disrupting the material exchange needed to sustain the embryo (Gu et al., 2002). However, the impact of *Procr* deletion on the embryo proper itself has been overlooked, mainly because Procr in the embryo proper was not detected by immunostaining until around E13.5, thus its action on vascular morphogenesis was deemed unlikely (Crawley et al., 2002). With our current findings on Procr as an early marker for endothelial progenitors, it is possible that the embryonic lethal phenotype seen in *Procr* homozygous knockout is not the sole result of placental fibrin deposition. Rather, embryonic vascular defects and placental clotting combined are likely responsible for the reported embryo lethality.

Intriguingly, deletion of Procr^{+} cells prior to HSC emergence (at E8.5) also impaired blood generation, as observed in the *Procr*^{CreERT2};*R26*^{DTA} line (Fig. 4). During embryonic development, blood cells and endothelium arise in close proximity. Using lineage-tracing (Jaffredo et al., 1998; Zovein et al., 2008) and time-lapse imaging (Bertrand et al., 2010; Boisset et al., 2010; Eilken et al., 2009; Lancrin et al., 2009) approaches, studies have demonstrated that blood progenitors are generated from endothelium through the process of endothelial-to-hematopoietic transition. Our scRNA-seq analysis also shows a hematopoietic lineage bifurcation at E8.25 from Procr^{+} ECs. Furthermore, when Procr^{+} cells were ablated at E8.5, embryos exhibited deformed vessels and loss of blood generation, suggesting the accompanied diminishment of hemogenic endothelium as a result. This is consistent with recent studies showing that cells primed to become HSCs display an endothelial signature that includes Procr (Hou et al., 2020; Zeng et al., 2019; Zhou et al., 2016).

In summary, we show that Procr expression marks the embryonic endothelial progenitors and demonstrate that Procr^{+} progenitors are indispensable for the establishment of the vasculature. In addition, we provide *in vivo* evidence to support the hypothesis

Development (2022) 149, dev200419. doi:10.1242/dev.200419

that Procr^{+} endothelial progenitors could also give rise to hematopoietic cells. These findings provide molecular cues for the enrichment of vessel-initiating progenitors, which could advance our understanding of the early cellular events in vascular morphogenesis and hematopoiesis.

MATERIALS AND METHODS

Experimental animals

Procr$^{mGFP\text{-}2A\text{-}lacZ}$, *Procr*^{CreERT2} and *Procr*^{Cre} strains were generated in our lab previously (Wang et al., 2018; Wang et al., 2020; Wang et al., 2021). Female mice of *Rosa26*$^{mTmG/+}$, *Rosa26*$^{DTA/+}$, *Rosa26*$^{tdTomato/+}$ (The Jackson Laboratory) were used in this study for lineage experiments. For induced lineage tracing and DTA-mediated cell-ablation experiments, after the observation of a virginal plug (E0.5), pregnancy was timed and the female received injection of 0.5 mg per 25 g body weight of TAM (Sigma-Aldrich) diluted in sunflower oil. Experimental procedures were approved by the Animal Care and Use Committee of Shanghai Institute of Biochemistry and Cell Biology, Chinese Academy of Sciences.

β-Galactosidase staining

Embryos were isolated and washed in cold PBS followed by incubation in ice-cold fixative (30 min up to E10.5, or 50 min for E11.5-E13.5; fixative contains 37% formaldehyde, 25% glutaraldehyde, 10% NP-40 dissolved in PBS) on a rocking platform. Whole embryos were washed twice in PBS for 20 min at room temperature. The β-galactosidase substrate [5 mM $K_3FE(CN)_6$, 5 mM $K_4Fe(CN)_6{\cdot}3H_2O$, 2 mM $MgCl_2$, 0.02% NP-40, 0.1% sodium deoxycholate and 1 mg/ml X-gal in PBS) was then added and the tissues incubated overnight at room temperature, shielded from light. Following staining, the tissues were washed twice in PBS for 20 min at room temperature. Embryos were serially dehydrated using glycerol, and stored in 80% glycerol at 4°C. Whole-embryo analysis of X-gal staining as shown in Fig. 1 and Fig. S2 was captured using an Olympus SZX16 stereo microscope.

Immunohistochemistry

Whole-embryo immunohistochemistry was prepared by fixing the entire embryo in ice-cold 4% paraformaldehyde for 2 h (up to E10.5). Fixed embryos were cryoprotected by immersion in 30% sucrose overnight at 4°C before being embedded in optimal cutting temperature compound (NEG-50, Thermo Scientific) and stored at −80°C. Frozen sections were prepared by air-drying and fixation for 45 min in cold 4% paraformaldehyde, followed by 20 min permeabilization in 0.1% Triton X-100 and 1 h blocking using 10% of the appropriate serum in PBS. Tissue sections were incubated with primary antibodies at 4°C overnight, followed by three PBS washes, 20 min each, incubation with secondary antibodies for 2 h at room temperature, and counterstaining with DAPI (Invitrogen, D1306). Representative images are shown in the figures. The primary antibodies used for immunofluorescence were: rat anti-mouse CD31 (1:50, BD Biosciences, clone MEC13.3), rabbit anti-mouse collagen type IV (1:200, Millipore, AB756P), mouse anti αSMA (1:1000, Sigma-Aldrich, A2547), rabbit anti-ERG (1:500, Abcam, ab92513), chicken anti-mouse GFP (1:1000, Invitrogen, A10262) and isolectin IB_4-488 (1:100, Invitrogen, I21411). The secondary antibodies used were: donkey anti-rat Cy3 (1:1000, Jackson ImmunoResearch, 712-165-150), goat anti-rat Alexa Fluor 488 (1:1000, Invitrogen, A-11006), goat anti-mouse Alexa Fluor 647 (1:1000, Invitrogen, A-21236) and donkey anti-goat Alexa Fluor 647 (1:1000, Invitrogen, A-21447). Confocal images were captured using a Leica DM6000 TCS/SP8 laser confocal microscope. All presented images were scanned as multiple layers at 1.2 µm thickness for each layer and *z*-stack processed to ensure correct colocalization of fluorescence signals.

Whole-mount embryo *in situ* hybridization

Digoxigenin-labeled riboprobes were designed and synthesized as previously described (Peng et al., 2016). In brief, both sense and antisense probe templates were generated from E8.0 mouse cDNA by PCR using gene-specific primers, with T7 promoter sequences (5′-TAATACGACTCACTATAGGGAGA-3′) added to the reverse primer. The PCR products were then purified and transcribed using the Roche DIG RNA labeling kit (Roche Applied Science) with T7 RNA polymerase. Whole-mount mRNA *in situ* hybridization on E7.0 mouse embryo was performed as described previously (Huang et al., 2010).

Flow cytometry

Timed embryos were dissected and dissociated with Accutase (StemPro™, A1110501) at 37°C. Cells were dissociated by 5 min gentle pipetting until a uniform cell solution was achieved. Single-cell suspensions were prepared by passing the digestion mix through a 40 µm nylon mesh. The following antibodies were used: FITC-conjugated CD45 (1:200, BioLegend, clone 30-F11), APC-conjugated CD31 (1:100, BD Pharmingen, clone MEC 13.3) and Procr (1:200, eBioscience, clone eBio1560) and streptavidin-v450 (1:500, eBioscience, 48-4317-82). Antibody incubation was performed on ice for 20-30 min in PBS with 5% fetal bovine serum (HyClone, Thermo Scientific). All analysis and sorting were performed using a FACSJazz (Becton Dickinson). The purity of sorted population was routinely checked and ensured to be >95%.

Single-cell collection and scRNA-seq library construction

Single-cell RNA-seq libraries were performed following previously described methods (Chen et al., 2017; Picelli et al., 2014). Briefly, single cells were lysed in the lysis buffer containing oligo-dT oligonucleotides to capture the polyadenylated RNA molecules, and reverse transcription was then performed with Superscript II reverse transcriptase (Invitrogen, 18064-014). After first-strand synthesis, cDNA was amplified with KAPA HiFi Hotstart ReadyMix (KAPA Biosystems) using IS-PCR primer for a total 18 cycles. The amplified cDNA was used for the quantitative real-time PCR assay with Stormstar SYBR green qPCR master mix (DBI Bioscience, DBI-143). Before RNA-seq library construction, the cDNA samples were purified with Agencourt Ampure XP beads (Beckman Coulter, A63881) on a Bravo automated liquid handling platform (Agilent) at the Chemical Biology Core Facility in Shanghai Institute of Biochemistry and Cell Biology. cDNA sequencing libraries were prepared using the TruePrep DNA Library Prep Kit V2 for Illumina® according to the manufacturer's instructions. Pair-end 150 bp sequencing was performed on a HiSeq X Ten platform at the Berry Genomics Co., Ltd (Beijing, China).

Analysis of scRNA-seq data

The sequencing quality of all raw sequencing data were evaluated by FastQC and were separately mapped to the mouse GRCm38 genome assemblies using HISAT2 (Pertea et al., 2016) using default settings. The mapping ratio was calculated based on the number of mapped reads and total reads for each sample. All mapped reads were processed by StringTie (Pertea et al., 2016) to quantify gene expression levels [measured as fragments per kilobase per million (FPKM)] using default parameters. Uniquely aligned reads were counted using the 'htseq-count' tool of HTSeq (Anders et al., 2015). Seurat 3 R package was used for cell filtering and data integration, analysis and visualization (Butler et al., 2018). To create Seurat object, cells that had at least 5000 detected genes were selected. Therefore, 60 cells were omitted (from 739 cells to 679 cells). For the analyses involving the E8.25 Flk1^{+} single-cell RNA-seq data from Pijuan-Sala et al. (2019), the same filtering standards were used for the Seurat object creation, and one cell was omitted out of 250 sequenced cells. For PC selection, differentially expressed genes were found by the 'vst' method and the top 5000 differentially expressed genes were selected for PCA analysis. PC selection was based on an elbow plot. Thirty PCs were used for dimensional reduction and cell clustering. For dimensional reduction, cell clustering and data display, dimensional reduction was performed using uniform manifold approximation and projection (UMAP). Cell clustering was based on shared-nearest neighbor method and the resolution was set to 3.0. Clusters were then put together as one cell type based on the similarity of the expression profiles and the marker genes expression. Heatmaps, dot plots and individual UMAP plots for the given genes were generated using the Seurat toolkit DoHeatmap, DotPlot and FeaturePlot functions, respectively. Monocle 2 R package (Qiu et al., 2017) was used for pseudotemporal analyses. All the cell types identified by Seurat were imported to Monocle 2

for the creation of a Monocle 2 CellDataSet object. In Monocle 2 analysis, we used the standard differentialGeneTest function and set the gene filter by qval<1e−70 to select the ordering genes. We performed 'plot_ordering_genes' analysis, and found that these selected ordering genes were suitable for trajectory analysis. We used the 'DDRTree' method for dimensional reduction and set the 'max_components' to 2 to generate one branching point. To reveal the difference of activated transcription factors, R package SCENIC v1.2.4 (Aibar et al., 2017) was used with default parameters.

Confocal microscopic imaging

Confocal images were captured using a Leica DM6000 TCS/SP8 laser confocal scanning microscope. All presented images were scanned as multiple layers at 1.0 µm thickness each layer and *z*-stack processed (i.e. multiple layers were stacked) to ensure correct colocalization of fluorescence signals. Whole embryo images were obtained using the Imaris 8.2.0 tiling function with 10% overlap between each neighboring view.

Quantification and statistical analysis

Unpaired Student's *t*-test was performed and *P*-values were calculated, with $P<0.05$ considered as statistically significant. When only two groups were compared, a two-sided Student's *t*-test was used. Data were analyzed and plotted using GraphPad Prism. For all experiments with error bars, s.e.m. was calculated to indicate the variation within each experiment.

Acknowledgements

We are grateful for the experimental support from Uli Schwarz Quantitative Biology Core Facility in PICB, CAS. We thank Dr Yujie Chen for assistance with confocal microscopy in this study.

Competing interests

The authors declare no competing or financial interests.

Author contributions

Conceptualization: Q.C.Y., N.J., Y.A.Z.; Methodology: Q.C.Y., L.B., Yingying Chen, Yujie Chen, G.P., G.C.; Validation: Q.C.Y., L.B.; Formal analysis: Q.C.Y., Yingying Chen, Y.A.Z.; Investigation: Q.C.Y., L.B., Yingying Chen, Yujie Chen, G.Y.; Resources: G.P., D.W., N.J.; Data curation: Q.C.Y., L.B., G.P., D.W., G.Y.; Writing - original draft: Q.C.Y.; Visualization: Yujie Chen; Supervision: N.J., Y.A.Z.; Project administration: Q.C.Y.; Funding acquisition: Q.C.Y., Y.A.Z.

Funding

This research was supported by grants from the National Natural Science Foundation of China (31830056 and 31861163006 to Y.A.Z.; 81873532 to Q.C.Y.), the Chinese Academy of Sciences (XDA16020200 to Y.A.Z.) and the National Key Research and Development Program of China (2020YFA0509002 to Y.A.Z.). Q.C.Y. is a member of the Youth Innovation Promotion Association of Chinese Academy of Sciences.

Data availability

The scRNA-seq datasets generated during this study have been deposited in The National Omics Data Encyclopedia (https://www.biosino.org/node/index) under accession number OEP001233.

Peer review history

The peer review history is available online at https://journals.biologists.com/dev/article-lookup/doi/10.1242/dev.200419.

Reference

Adams, R. H. and Alitalo, K. (2007). Molecular regulation of angiogenesis and lymphangiogenesis. *Nat. Rev. Mol. Cell Biol.* **8**, 464-478. doi:10.1038/nrm2183

Aibar, S., Gonzalez-Blas, C. B., Moerman, T., Huynh-Thu, V. A., Imrichova, H., Hulselmans, G., Rambow, F., Marine, J. C., Geurts, P., Aerts, J. et al. (2017). SCENIC: single-cell regulatory network inference and clustering. *Nat. Methods* **14**, 1083-1086. doi:10.1038/nmeth.4463

Anders, S., Pyl, P. T. and Huber, W. (2015). HTSeq–a Python framework to work with high-throughput sequencing data. *Bioinformatics* **31**, 166-169. doi:10.1093/bioinformatics/btu638

Balazs, A. B., Fabian, A. J., Esmon, C. T. and Mulligan, R. C. (2006). Endothelial protein C receptor (CD201) explicitly identifies hematopoietic stem cells in murine bone marrow. *Blood* **107**, 2317-2321. doi:10.1182/blood-2005-06-2249

Bertrand, J. Y., Chi, N. C., Santoso, B., Teng, S., Stainier, D. Y. and Traver, D. (2010). Haematopoietic stem cells derive directly from aortic endothelium during development. *Nature* **464**, 108-111. doi:10.1038/nature08738

Boisset, J. C., van Cappellen, W., Andrieu-Soler, C., Galjart, N., Dzierzak, E. and Robin, C. (2010). In vivo imaging of haematopoietic cells emerging from the mouse aortic endothelium. *Nature* **464**, 116-120. doi:10.1038/nature08764

Buschmann, I., Pries, A., Styp-Rekowska, B., Hillmeister, P., Loufrani, L., Henrion, D., Shi, Y., Duelsner, A., Hoefer, I., Gatzke, N. et al. (2010). Pulsatile shear and Gja5 modulate arterial identity and remodeling events during flow-driven arteriogenesis. *Development* **137**, 2187-2196. doi:10.1242/dev.045351

Butler, A., Hoffman, P., Smibert, P., Papalexi, E. and Satija, R. (2018). Integrating single-cell transcriptomic data across different conditions, technologies, and species. *Nat. Biotechnol.* **36**, 411-420. doi:10.1038/nbt.4096

Carmeliet, P. (2003). Angiogenesis in health and disease. *Nat. Med.* **9**, 653-660. doi:10.1038/nm0603-653

Chen, J., Suo, S., Tam, P. P., Han, J. J., Peng, G. and Jing, N. (2017). Spatial transcriptomic analysis of cryosectioned tissue samples with Geo-seq. *Nat. Protoc.* **12**, 566-580. doi:10.1038/nprot.2017.003

Cheng, T., Liu, D., Griffin, J. H., Fernandez, J. A., Castellino, F., Rosen, E. D., Fukudome, K. and Zlokovic, B. V. (2003). Activated protein C blocks p53-mediated apoptosis in ischemic human brain endothelium and is neuroprotective. *Nat. Med.* **9**, 338-342. doi:10.1038/nm826

Clements, W. K. and Traver, D. (2013). Signalling pathways that control vertebrate haematopoietic stem cell specification. *Nat. Rev. Immunol.* **13**, 336-348. doi:10.1038/nri3443

Coultas, L., Chawengsaksophak, K. and Rossant, J. (2005). Endothelial cells and VEGF in vascular development. *Nature* **438**, 937-945. doi:10.1038/nature04479

Crawley, J. T., Gu, J. M., Ferrell, G. and Esmon, C. T. (2002). Distribution of endothelial cell protein C/activated protein C receptor (EPCR) during mouse embryo development. *Thromb. Haemost.* **88**, 259-266. doi:10.1055/s-0037-1613196

Eichmann, A., Yuan, L., Moyon, D., Lenoble, F., Pardanaud, L. and Breant, C. (2005). Vascular development: from precursor cells to branched arterial and venous networks. *Int. J. Dev. Biol.* **49**, 259-267. doi:10.1387/ijdb.041941ae

Eilken, H. M., Nishikawa, S. and Schroeder, T. (2009). Continuous single-cell imaging of blood generation from haemogenic endothelium. *Nature* **457**, 896-900. doi:10.1038/nature07760

Ema, M. and Rossant, J. (2003). Cell fate decisions in early blood vessel formation. *Trends Cardiovas. Med.* **13**, 254-259. doi:10.1016/S1050-1738(03)00105-1

Esmon, C. T. (2001). Protein C anticoagulant pathway and its role in controlling microvascular thrombosis and inflammation. *Crit. Care Med.* **29**, S48-S51; discussion 51-42.

Esmon, C. T., Gu, J. M., Xu, J., Qu, D. F., Stearns-Kurosawa, D. J. and Kurosawa, S. (1999). Regulation and functions of the protein C anticoagulant pathway. *Haematologica* **84**, 363-368.

Fares, I., Chagraoui, J., Lehnertz, B., MacRae, T., Mayotte, N., Tomellini, E., Aubert, L., Roux, P. P. and Sauvageau, G. (2017). EPCR expression marks UM171-expanded CD34(+) cord blood stem cells. *Blood* **129**, 3344-3351. doi:10.1182/blood-2016-11-750729

Fukudome, K. and Esmon, C. T. (1995). Molecular cloning and expression of murine and bovine endothelial cell protein C/activated protein C receptor (EPCR). The structural and functional conservation in human, bovine, and murine EPCR. *J. Biol. Chem.* **270**, 5571-5577.

Griffin, J. H., Zlokovic, B. V. and Mosnier, L. O. (2012). Protein C anticoagulant and cytoprotective pathways. *Int. J. Hematol.* **95**, 333-345. doi:10.1007/s12185-012-1059-0

Gu, J. M., Crawley, J. T., Ferrell, G., Zhang, F., Li, W., Esmon, N. L. and Esmon, C. T. (2002). Disruption of the endothelial cell protein C receptor gene in mice causes placental thrombosis and early embryonic lethality. *J. Biol. Chem.* **277**, 43335-43343. doi:10.1074/jbc.M207538200

Hou, S., Li, Z., Zheng, X., Gao, Y., Dong, J., Ni, Y., Wang, X., Li, Y., Ding, X., Chang, Z. et al. (2020). Embryonic endothelial evolution towards first hematopoietic stem cells revealed by single-cell transcriptomic and functional analyses. *Cell Res.* **30**, 376-392. doi:10.1038/s41422-020-0300-2

Huang, C., Xiang, Y., Wang, Y., Li, X., Xu, L., Zhu, Z., Zhang, T., Zhu, Q., Zhang, K., Jing, N. et al. (2010). Dual-specificity histone demethylase KIAA1718 (KDM7A) regulates neural differentiation through FGF4. *Cell Res.* **20**, 154-165. doi:10.1038/cr.2010.5

Jaffredo, T., Gautier, R., Eichmann, A. and Dieterlen-Lievre, F. (1998). Intraaortic hemopoietic cells are derived from endothelial cells during ontogeny. *Development* **125**, 4575-4583. doi:10.1242/dev.125.22.4575

Lancrin, C., Sroczynska, P., Stephenson, C., Allen, T., Kouskoff, V. and Lacaud, G. (2009). The haemangioblast generates haematopoietic cells through a haemogenic endothelium stage. *Nature* **457**, 892-895. doi:10.1038/nature07679

Li, Z. A., Lan, Y., He, W. Y., Chen, D. B., Wang, J., Zhou, F., Wang, Y., Sun, H. Y., Chen, X. D., Xu, C. H. et al. (2012). Mouse embryonic head as a site for hematopoietic stem cell development. *Cell Stem Cell* **11**, 663-675. doi:10.1016/j.stem.2012.07.004

Mohan Rao, L. V., Esmon, C. T. and Pendurthi, U. R. (2014). Endothelial cell protein C receptor: a multiliganded and multifunctional receptor. *Blood* **124**, 1553-1562. doi:10.1182/blood-2014-05-578328

Peng, G., Suo, S., Chen, J., Chen, W., Liu, C., Yu, F., Wang, R., Chen, S., Sun, N., Cui, G. et al. (2016). Spatial transcriptome for the molecular annotation of lineage fates and cell identity in mid-gastrula mouse embryo. *Dev. Cell* **36**, 681-697. doi:10.1016/j.devcel.2016.02.020

Pertea, M., Kim, D., Pertea, G. M., Leek, J. T. and Salzberg, S. L. (2016). Transcript-level expression analysis of RNA-seq experiments with HISAT, StringTie and Ballgown. *Nat. Protoc.* **11**, 1650-1667. doi:10.1038/nprot.2016.095

Picelli, S., Faridani, O. R., Bjorklund, A. K., Winberg, G., Sagasser, S. and Sandberg, R. (2014). Full-length RNA-seq from single cells using Smart-seq2. *Nat. Protoc.* **9**, 171-181. doi:10.1038/nprot.2014.006

Pijuan-Sala, B., Griffiths, J. A., Guibentif, C., Hiscock, T. W., Jawaid, W., Calero-Nieto, F. J., Mulas, C., Ibarra-Soria, X., Tyser, R. C. V., Ho, D. L. L. et al. (2019). A single-cell molecular map of mouse gastrulation and early organogenesis. *Nature* **566**, 490-495. doi:10.1038/s41586-019-0933-9

Qiu, X., Mao, Q., Tang, Y., Wang, L., Chawla, R., Pliner, H. A. and Trapnell, C. (2017). Reversed graph embedding resolves complex single-cell trajectories. *Nat. Methods* **14**, 979-982. doi:10.1038/nmeth.4402

Rossant, J. and Cross, J. C. (2001). Placental development: lessons from mouse mutants. *Nat. Rev. Genet.* **2**, 538-548. doi:10.1038/35080570

Swift, M. R., Pham, V. N., Castranova, D., Bell, K., Poole, R. J. and Weinstein, B. M. (2014). SoxF factors and Notch regulate nr2f2 gene expression during venous differentiation in zebrafish. *Dev. Biol.* **390**, 116-125. doi:10.1016/j.ydbio.2014.03.018

Wang, D., Cai, C., Dong, X., Yu, Q. C., Zhang, X. O., Yang, L. and Zeng, Y. A. (2015). Identification of multipotent mammary stem cells by protein C receptor expression. *Nature* **517**, 81-84. doi:10.1038/nature13851

Wang, D., Liu, C., Wang, J., Jia, Y., Hu, X., Jiang, H., Shao, Z. M. and Zeng, Y. A. (2018). Protein C receptor stimulates multiple signaling pathways in breast cancer cells. *J. Biol. Chem.* **293**, 1413-1424. doi:10.1074/jbc.M117.814046

Wang, D., Wang, J., Bai, L., Pan, H., Feng, H., Clevers, H. and Zeng, Y. A. (2020). Long-term expansion of pancreatic islet organoids from resident Procr(+) progenitors. *Cell* **180**, 1198-1211.

Wang, J., Chu, K., Wang, Y., Li, J., Fu, J., Zeng, Y. A. and Li, W. (2021). Procr-expressing granulosa cells are highly proliferative and are important for follicle development. *iScience* **24**, 102065. doi:10.1016/j.isci.2021.102065

Ye, H., Wang, X., Li, Z., Zhou, F., Li, X., Ni, Y., Zhang, W., Tang, F., Liu, B. and Lan, Y. (2017). Clonal analysis reveals remarkable functional heterogeneity during hematopoietic stem cell emergence. *Cell Res.* **27**, 1065-1068. doi:10.1038/cr.2017.64

Yu, Q. C., Song, W., Wang, D. and Zeng, Y. A. (2016). Identification of blood vascular endothelial stem cells by the expression of protein C receptor. *Cell Res.* **26**, 1079-1098. doi:10.1038/cr.2016.85

Zeng, Y., He, J., Bai, Z., Li, Z., Gong, Y., Liu, C., Ni, Y., Du, J., Ma, C., Bian, L. et al. (2019). Tracing the first hematopoietic stem cell generation in human embryo by single-cell RNA sequencing. *Cell Res.* **29**, 881-894. doi:10.1038/s41422-019-0228-6

Zhou, F., Li, X., Wang, W., Zhu, P., Zhou, J., He, W., Ding, M., Xiong, F., Zheng, X., Li, Z. et al. (2016). Tracing haematopoietic stem cell formation at single-cell resolution. *Nature* **533**, 487-492. doi:10.1038/nature17997

Zovein, A. C., Hofmann, J. J., Lynch, M., French, W. J., Turlo, K. A., Yang, Y., Becker, M. S., Zanetta, L., Dejana, E., Gasson, J. C. et al. (2008). Fate tracing reveals the endothelial origin of hematopoietic stem cells. *Cell Stem Cell* **3**, 625-636. doi:10.1016/j.stem.2008.09.018

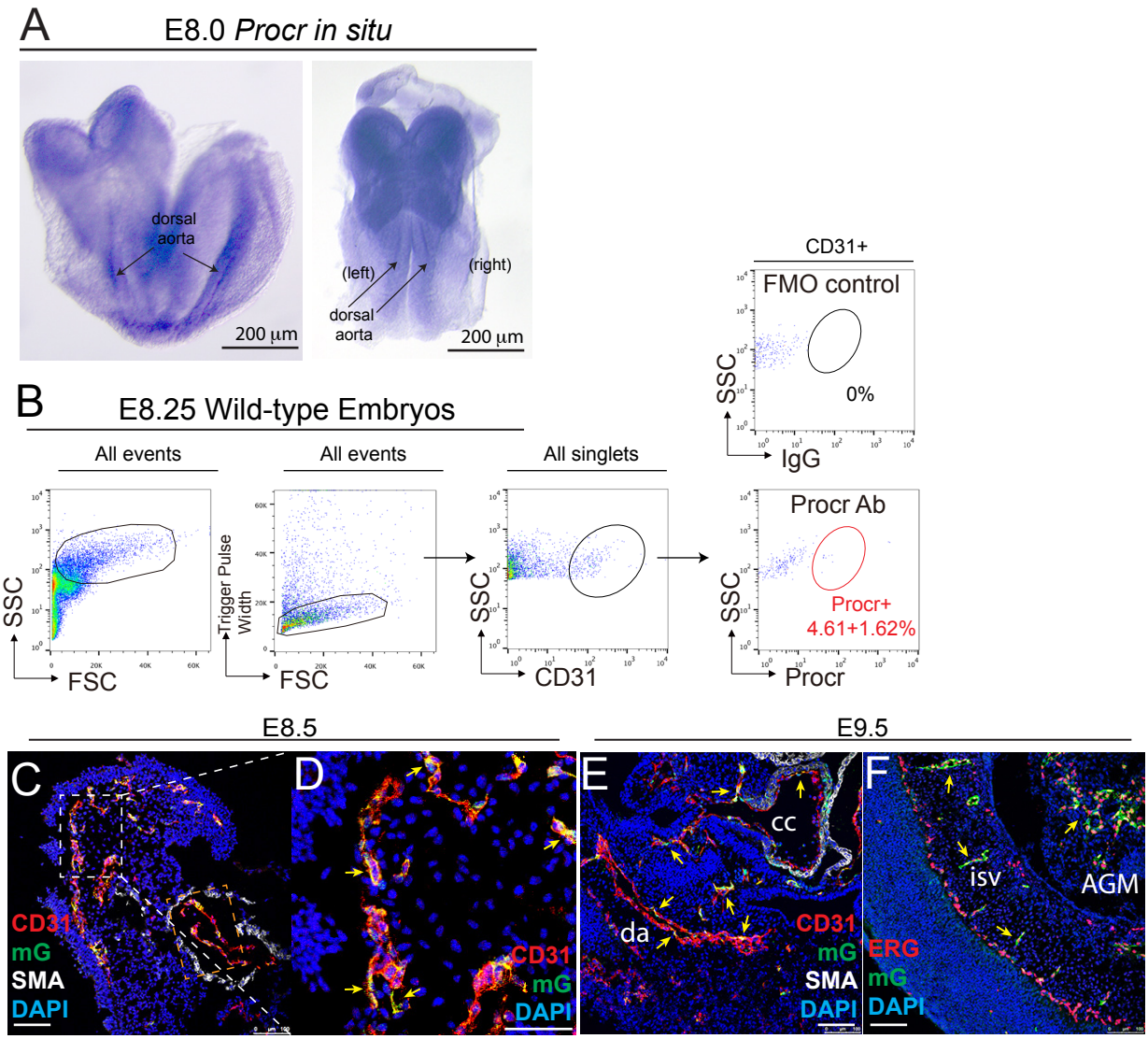

Fig. S1. Procr expression pattern during embryonic development.

(A) Whole-mount in situ hybridization result of Procr expression on E8.0 wild-type embryos. Dense positive staining was observed on dorsal aortae, consistent with the staining result from *Procr*$^{mGFP\text{-}2A\text{-}LacZ}$ reporter embryos. **(B)** FACS analysis on E8.25 WT embryo endothelium (CD31+) indicate a subpopulation of Procr+ ECs. Data in FACS plots are from at least 5 embryos and is presented as mean ± Standard error of the mean (S.E.M). **(C-D)** Immunohistochemistry of E8.5 *Procr*$^{mGFP\text{-}2A\text{-}LacZ}$ embryo section indicating the presence of Procr+ ECs (indicated as mG+) on the forming aorta (out-lined by CD31, white box) and within cardiac cavity (orange box). White boxed area is enlarged at right **(D)**. Procr+ cells indicated by yellow arrows. mG, mGFP. **(E-F)** Immu-nohistochemistry of E9.5 *Procr*$^{mGFP\text{-}2A\text{-}LacZ}$ embryo showing Procr+ ECs on multiple vascular beds (ERG labels EC nuecli), including the aorta and cardiac cavity (**E**, yellow arrows) as well as the forming intersomatic vessels and vessel plexus surrounding aorta-gonald-mesonephro (AGM) region (**F**, yellow arrows). da: dorsal aorta, cc: cardi-ac cavity, isv: intersomatic vessels. **C-F**, Scale bars, 50μm.

Development • Supplementary information

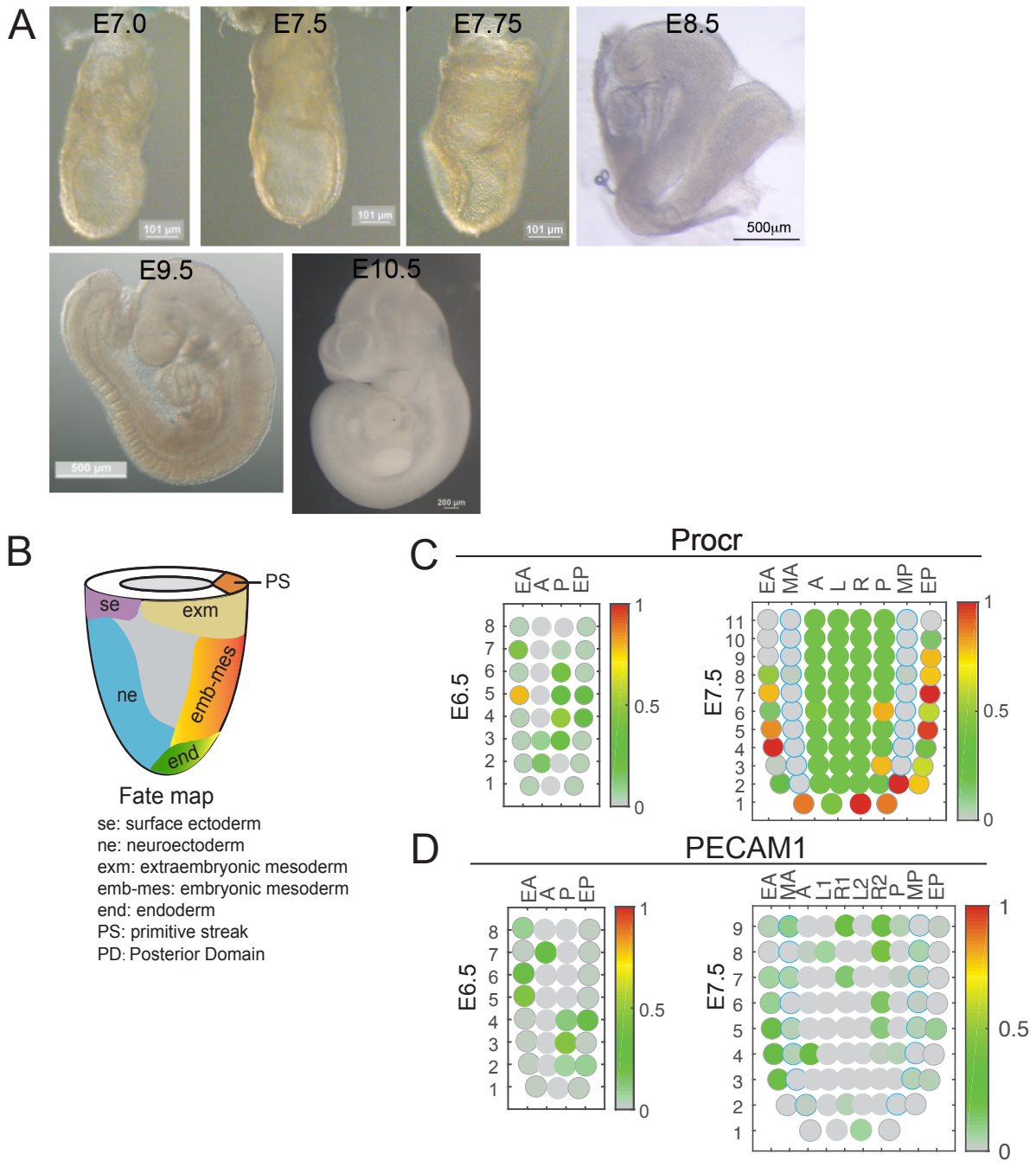

Fig. S2. Expression of Procr during early embryonic development.

(A) X-gal staining of the wild-type embryos. Scale bars as indicated in each image. Embryos from the same pregnant female were harvested and stained simultaneously. Embryos from more than 3 pregnant female mice were analyzed for each time point. **(B)** Illustration of embryonic fate map during gastrulation. **(C-D)** Cornplot showing the spatial expression pattern of Procr and PECAM1(CD31) within E6.5 and E7.5 embryos. EA: anterior endoderm; MA: anterior mesoderm; A: anterior; L: left lateral; R: right lateral; P: posterior; MP: posterior mesoderm; EP: posterior endoderm.

Development • Supplementary information

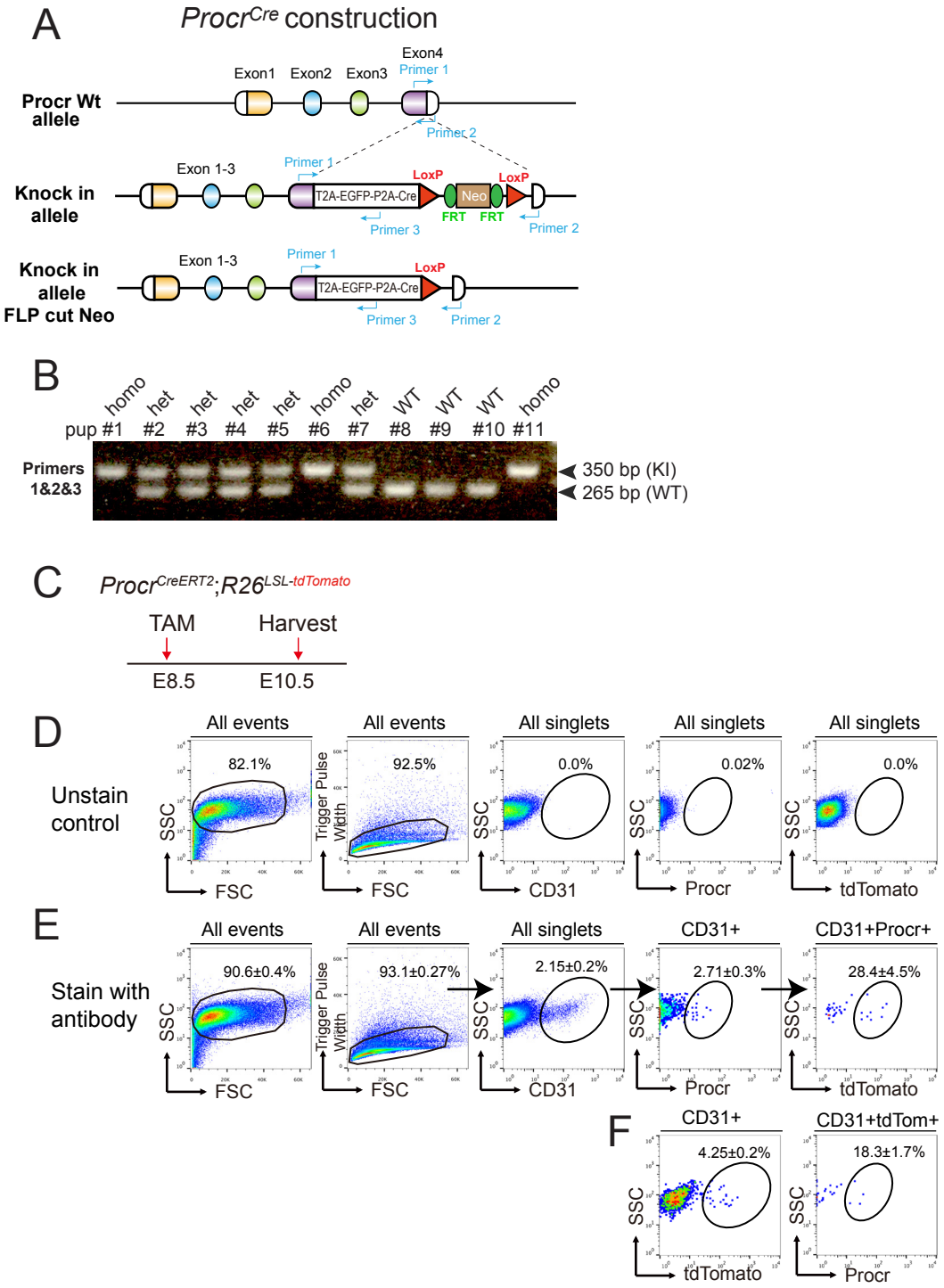

Fig. S3. Generation of the ProcrCre knock-in mouse.

(A) Targeting strategy to generate the *Procr*^{Cre} knock-in (KI) mouse. Designs of the genotyping primers are as indicated. **(B)** Genotyping PCR indicating the positive allele carrying a 350bp band. Mating between two heterozygous parents resulted in proper distribution of wild type, heterozygotes and homozygotes as Mendel's law of segregation. **(C)** Induction strategy of *Procr*^{CreERT2};*R26*$^{LSL\text{-}tdTomato}$ mouse. **(D-F)** FACS analyses on *Procr*^{CreERT2};*R26*$^{LSL\text{-}tdTomato}$ embryos after 2 days induction reflecting the labeling efficiency **(D)** and progeny generation **(F)**. **C-F**; data from more than 5 embryos were collected.

Development • Supplementary information

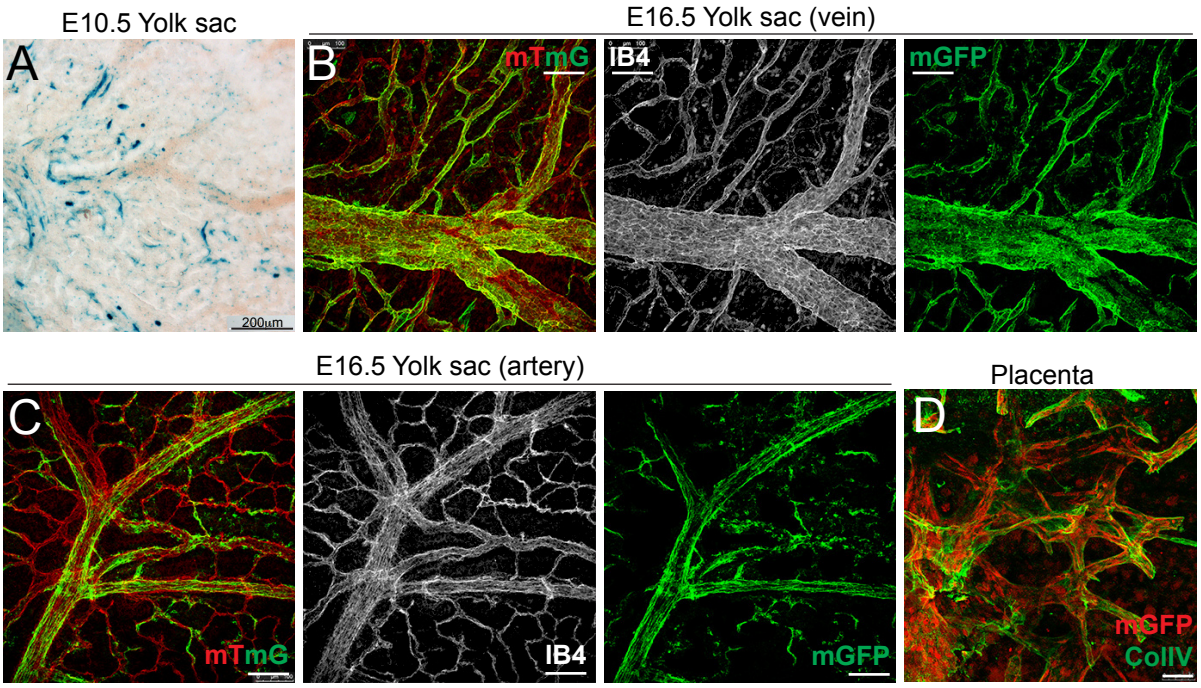

Fig. S4. Procr+ cells contribute to yolk sac and placental vasculature.
(A) Representative image of X-gal staining on E10.5 *Procr*$^{mGFP\text{-}2A\text{-}LacZ}$ shows Procr+ cells on yolk sac vessels. Scale bar, 200 μm. More than 5 embryos were examined.**(B-C)** At E16.5, yolk sac vessels of *Procr*^{Cre};*R26*^{mTmG} embryo, both veins **(B)** and arteries **(C)** were heavily decorated with mGFP signals, suggesting that they were derived from initially labeled Procr+ cells. Isolectin B4 (IB4, identifies endothelial lining) was used to label endothelial layer of vessels. **(D)** Procr+ cells also gave rise to the endothelial lining of labyrinth vessels inside the placenta. ColIV, Collagen IV. Scale bars, 50 μm. More than 5 yolk sac and placenta-attached embryos were harvested lineage tracing.

Development • Supplementary information

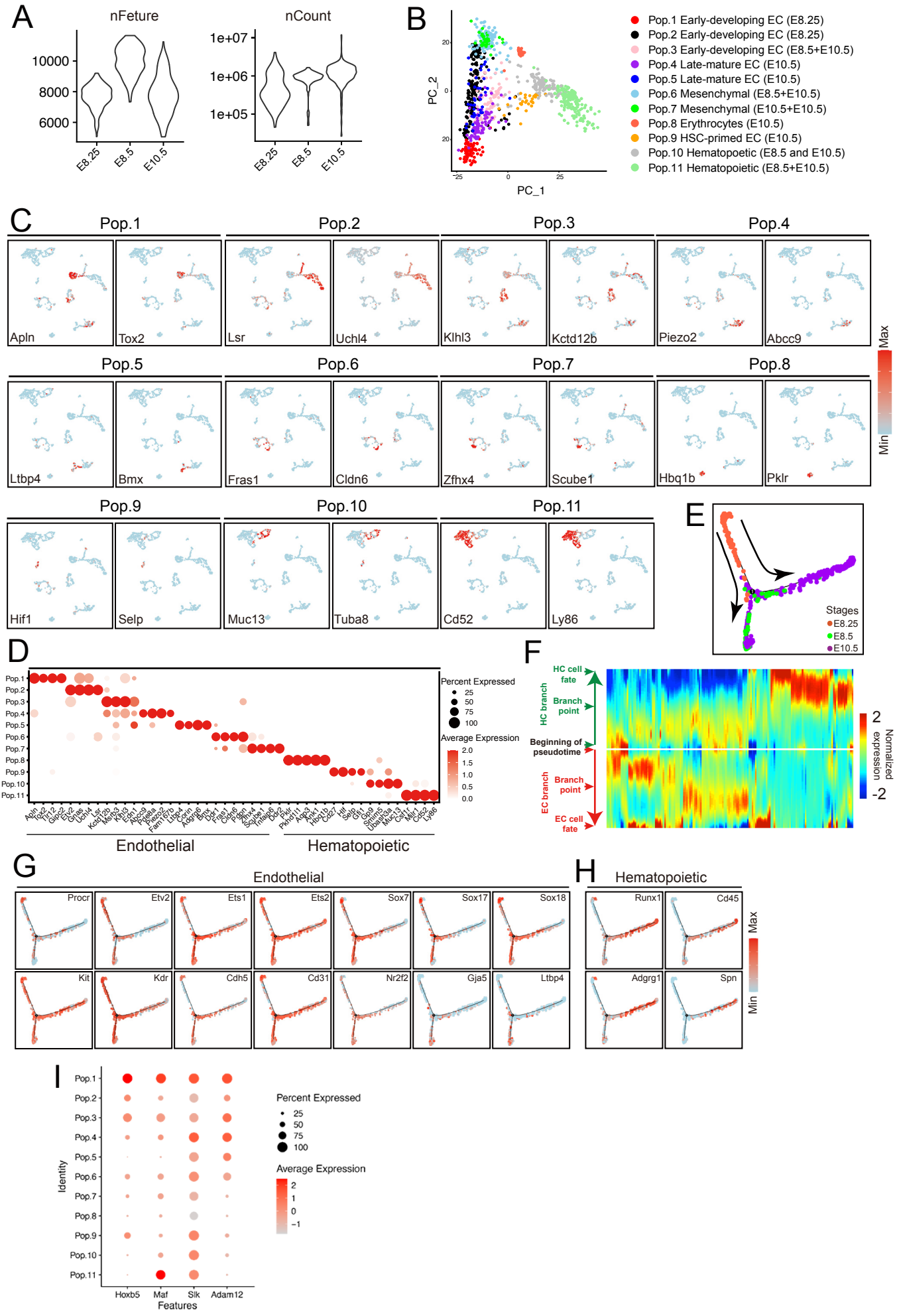

Development • Supplementary information

Fig. S5. scRNA-seq reveals Procr+ progenitors give rise to both endothelial and hematopoi-etic lineage.

(A) Quality metrics for the scRNA-seq data. Distributions of the number of genes detected per cell
(left) and the number of counts per cell (right) are shown. **(B)** PCA analyses of all cells from E8.25, E8.5 and E10.5 batches. **(C)** Individual gene UMAP plots showing the expression levels and distribu-tion of representative marker genes of each cluster. The colors ranging from blue to red indicate low to high relative gene expression levels. **(D)** Dot plot for signature genes of each cluster. The shadings denote average expression levels and the sizes of dots denote fractional expression. **(E)** Develop-mental trajectory of cells produced by Monocle 2. The colors denote cell stage. **(F)** The gene branched heatmap depicting the expression of genes along each branch in pseudotime. An indepen-dent expression pattern is calculated across the entire pseudotime trajectory for each branch. There-fore, the portion of the trajectory before the branch point is displayed for each branch separately. Genes are clustered based on expression pattern across pseudotime. **(G-H)** Individual gene expres-sion on pseudotime trajectory of known endothelial **(G)** and hematopoietic **(H)** cell types. The colors ranging from blue to red indicate low to high relative gene expression levels. **(I)** Dot plot for expres-sion pattern of *Hoxb5, Maf, Slk* and *Adam12* in different clusters. The shadings denote average expression levels and the sizes of dots denote fractional expression.

Development • Supplementary information

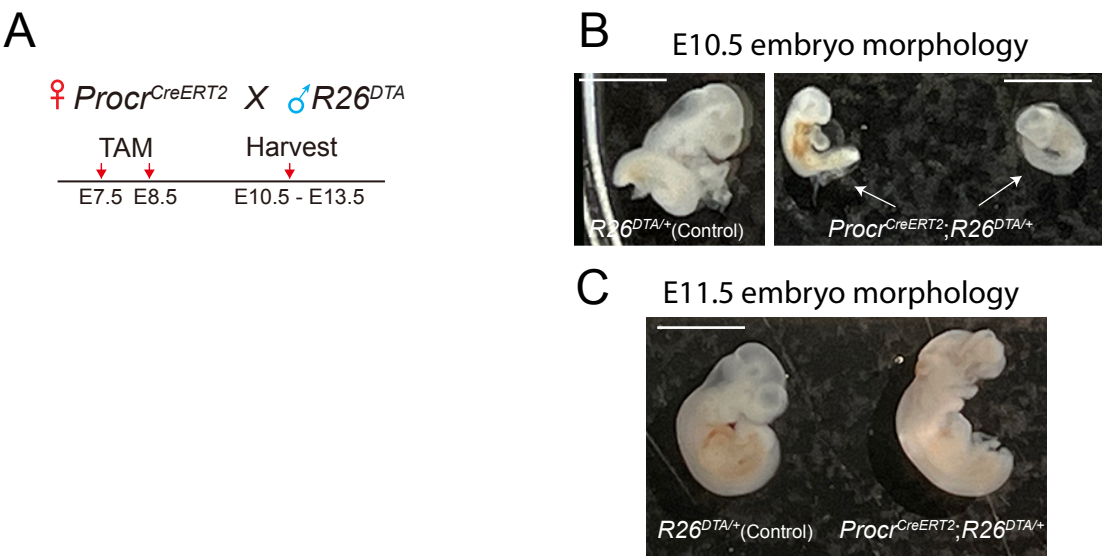

Fig. S6. Ablation of Procr+ cells cause embryonic lethality.
(A) Schematic illustration of Procr+ cell ablation strategy. Tamoxifen (TAM) was administered on E7.5 and E8.5 through maternal peritoneal injection, and the uterus was dissected for embryo morphology analysis. **(B-C)** Representative images of the dissected embryos from E10.5 **(B)** and E11.5 **(C)**. Scale bars, 500 μm. Targeted ablation experiments were performed in at least three pregnant female mice for each harvesting time point.

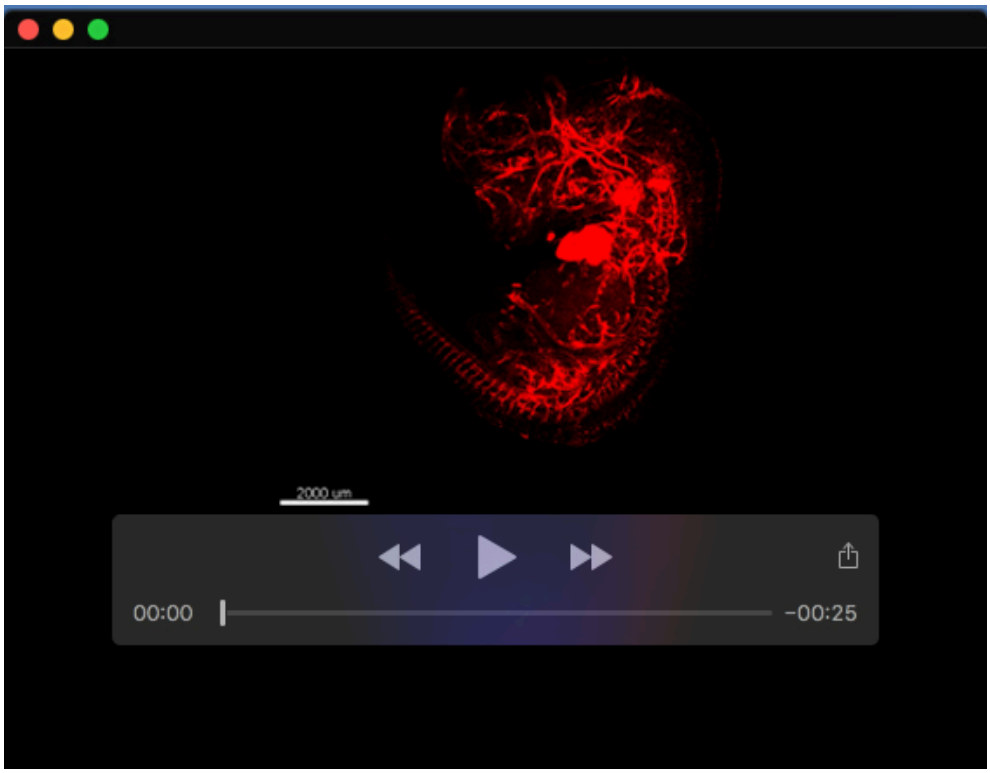

Movie 1. Whole embryo scanning of E12.5 *ProcrCre;R26LSL-tdTomato.*

Development • Supplementary information